The binding affinity of monoalkyl phosphinic acid ligands towards nanocrystal surfaces

Evert Dhaene,[1,2] Simon Coppenolle,[1] Loren Deblock,[1] Klaartje De Buysser,[1] Jonathan De Roo[2*]

[1] Department of Chemistry, Ghent University, Gent B-9000, Belgium

[2] Department of Chemistry, University of Basel, Basel CH-4058, Switzerland

* Corresponding author: Jonathan De Roo, Jonathan.DeRoo@unibas.ch

Abstract

We recently introduced monoalkyl phosphinic acids as a ligand class for nanocrystal synthesis. Their metal salts have interesting reactivity differences with respect to metal carboxylates and phosphonates, and provide cleaner work-up compared to phosphonates. However, there is little known about the surface chemistry of nanocrystals with monoalkyl phosphinate ligands. Here, we probe the relative binding affinity of monoalkyl phosphinate ligands with respect to other X-type ligands. We perform competitive ligand exchange reactions with carboxylate and phosphonate ligands at the surface of HfO_2, CdSe, and ZnS nanocrystals. We monitor the ligand shell composition by solution ^{1}H and ^{31}P NMR spectroscopy. Using a monoalkyl phosphinic acid with an ether functionality, we gain an additional NMR signature, apart from the typical alkene resonance in oleic acid and oleylphosphonic acid. We find that carboxylate ligands are easily exchanged upon exposure to monoalkyl phosphinic acids, whereas an equilibrium is reached between monoalkyl phosphinates and phosphonates, slightly in the favour of phosphonate (K = 2). Phosphinic acids have thus an intermediate binding affinity between carboxylic acids and phosphonic acids for all nanocrystals studied. These results enable the sophisticated use of monoalkyl phosphinic acids for nanocrystal synthesis and for post-synthetic surface engineering.

Keywords

nanocrystals, ligands, phosphinic acids, surface chemistry

Introduction

Colloidal nanocrystals (NCs) are an interesting materials class with a high surface-to-volume ratio.[1] Their physical and chemical properties depend on both the inorganic core and the ligand-capped surface. The ligand shell often consists of organic molecules providing colloidal stability/solubility.[2-7] Ligands can influence the electronic structure and optical properties of the NCs.[8] Without ligands, the atoms at the surface are coordinatively unsaturated, potentially causing electronic states within the band gap of semiconductor nanocrystals.[9-11] These trap states can accept either electrons or holes and thus quench the photoluminescence quantum yield. Manipulating the NC surface is thus essential to implement these hybrid nanomaterials into their various applications.

Surface manipulation is achieved by ligand exchange reactions. For example, organic ligands are often exchanged with inorganic ligands for applications in devices such as field effect transistors, photodetectors, photovoltaic devices, thermoelectric, and photoelectrocatalytic materials.[12, 13] However, these manipulations cannot be accomplished without understanding the ligand-NC bond. The covalent bond classification provides a framework for describing metal-ligand bonds and has also been used to describe NC-ligand bonds.[3, 4, 14] The number of electrons that a neutral ligand contributes to the bonding orbital determines the ligand type: two (L), one (X), or zero (Z). L-type ligands are thus donors of an electron-pair, and are equivalent to Lewis bases. Z-type ligands are neutral electron-pair acceptors, and equivalent to Lewis acids. X-type ligands are single electron donors in their neutral form. In an ionic model, they are usually anions (carboxylates, chlorides, etc.) but they can also be cations (protons).[15] In nonpolar solvents, the total colloidal object should be electrically neutral, while in polar solvents this restriction is absent.[16] In nonpolar solvents, X-type ligands either occur in ion pairs,[15, 17] or the charge is compensated by the nanocrystal core.[8, 18] Apart from providing a

framework of thought, the classification of ligands allows to predict or rationalize ligand exchange processes.[19]

Significant effort has been devoted to quantifying ligand exchange reactions. Not surprisingly, an equilibrium is observed for different ligands with the same binding group, e.g., carboxylate ligands are in equilibrium with most other carboxylic acids.[20-29] Interestingly, the driving force for X-type ligand exchange in nonpolar solvents is often the proton transfer from the incoming pro-ligand to the surface-bound ligand.[30] Regular carboxylate ligands ($pK_a \approx 4.75$) are quantitatively exchanged for a stronger acid such as phosphonic acids ($pK_a \approx 1.1 – 2.3$),[20-22, 31-36] trifluoroacetic acid ($pK_a \approx 0.5$),[36-38] or hydrochloric acid ($pK_a \approx -8$).[39] The reverse reaction (e.g., chloride is replaced by carboxylate) is observed when a base (e.g, an alkylamine) is added.[23, 30, 40] Under such basic conditions, the proton transfer is no longer part of the ligand exchange. Due to the higher intrinsic binding affinity of the carboxylate anion, chloride is replaced by carboxylate. An alkylammonium chloride salt is formed as a by-product.

In addition to proton transfer, other factors also play a role in X-type exchange. Steric bulk can hamper ligand exchange,[41] multidentate ligands can enhance the binding affinity,[42-44] and the ligand solubility can also steer the exchange reaction.[2, 16] The binding enthalpy of an X-type ligand can be particularly high for certain surfaces while low for other surfaces, due to chemical compatibility. For example, thiols have a high affinity for the surface of metal chalcogenide or metallic NCs, but are generally poor ligands for metal oxides.[20, 21, 24, 40, 45-49] Finally, a ligand exchange reaction can be forced by the formation of energetically favourable by-products. For example, the strong silicon-oxygen bond drives the exchange reaction from phosphonate to chloride by addition of trimethylsilyl chloride.[37, 50-54]

It thus appears the literature is quite complete regarding X-type ligand exchange that involves carboxylates and phosphonates, but there are no reports on surface chemistry with monoalkyl

phosphinic acids. This is not surprising since monoalkyl phosphinic acids were only recently introduced as ligand class for nanocrystal synthesis.[37] Dialkyl phosphinic acids have only been sparsely used in nanocrystal synthesis,[55-59] and typically do not bind to the nanocrystal surface due to sterical hindrance.[41]

Nuclear magnetic resonance (NMR) spectroscopy is one of the most suitable methods for probing ligand exchanges on the NC surface.[60] NMR spectroscopy has the ability to distinguish free from bound ligands, and allows for identification and quantification of the bound ligands.[61] Broadened resonances are inherent to ligands bound to a NC surface, and are used as an important diagnostic.[60] The broadening is homogeneous (slow T_2 relaxation) and heterogeneous (incomplete solvation) in nature, and depends on the nanocrystal size.[60] Advanced methods such as diffusion-ordered spectroscopy (DOSY) are used to probe the dynamics of ligand binding.[61] On the other hand, isothermal titration calorimetry has been recently used as a powerful, complementary technique to investigate (equilibrium) ligand exchange reactions.[6, 22, 32, 62, 63] It has the advantage of providing direct thermodynamic data by measuring accurately small heat changes. It does not provide the composition of the ligand shell or nor does it identify free ligands in solution.[22]

In this study, we investigate X-type ligand exchanges with monoalkyl phosphinic acids on both metal oxide (HfO_2) and metal chalcogenide (CdSe and ZnS) NCs. Given their intermediate acidity, monoalkyl phosphinic acids ($pK_a \approx 3.08$) are expected to bind to surfaces with an affinity between carboxylic and phosphonic acids.[37, 64] We designed two sets of exchange experiments to test this hypothesis. A first exchange reaction is carefully monitored by titrating oleate capped NCs with *6*-(hexyloxy)hexylphosphinic acid. After complete exchange and purification of the phosphinate capped NCs, a second titration is performed with oleylphosphonic acid. Using solution NMR spectroscopy, we quantify the X-for-X ligand exchanges via the alkene resonance of the oleyl chain of the carboxylic and phosphonic acid,

and the ether resonance of the monoalkyl phosphinic acid. The monoalkyl phosphinic acids quantitatively displace carboxylate ligands and are in equilibrium with phosphonates (although phosphonate binding is favoured). These results show that monoalkyl phosphinic acids are suitable reagents to efficiently functionalize NC surfaces.

Results and Discussion

Synthesis of monoalkyl phosphinic and phosphonic acid. To synthesize suitable monoalkyl phosphinic acid ligands for nanocrystals, we recently adopted two main methods.[37] The synthetic route reported by Deprèle *et al.* is applied for saturated monoalkyl phosphinic acids.[37, 65] The more complex phosphinic acids are synthesized according to Scheme 1.[37, 66] We synthesize here the previously unreported *6*-(hexyloxy)hexylphosphinic acid for our NMR investigations. As shown by Yamashita *et al*., the ether functionality provides a distinct NMR resonance, separate from the typical alkene resonance in oleyl chains.[28] Compared to the relatively short ligands with terminal alkenes that are typically used for monitoring ligand exchange reactions,[20, 30, 67, 68] the ether ligand features a better separation from the oleyl NMR resonances (rendering quantification more precise) and both the ligand and the nanocrystal-ligand construct have a higher solubility.

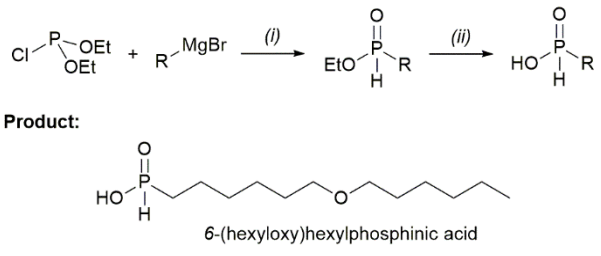

Scheme 1. Method to synthesize *6*-(hexyloxy)hexylphosphinic acid. Conditions: (i) overnight at 50 °C in dry THF, then 2h at room temperature in conc. HCl and water. (ii) 1.15 eq. of TMS-Br, overnight in dry DCM, then dry MeOH, 6h, 40 °C.

Earlier, we also reported a general route to synthesize alkylphosphonic acids.[33] To synthesize oleylphosphonic acid for quantitative ^{1}H NMR titrations, we choose here to start from oleic acid, not from oleyl alcohol, since the latter is contaminated with *trans* isomers. First, oleic acid is reduced to oleyl alcohol, according to the procedure of Sytniczuk *et al.*[37, 69] The Appel reaction converts the alcohol in the corresponding bromide.[70] Oleyl bromide is converted by a Michaelis-Becker reaction into the diethylphosphonate ester,[71] which is finally hydrolysed to oleylphosphonic acid.[72] Our final product is a white solid at room temperature instead of the previously reported viscous colourless liquid.[33]

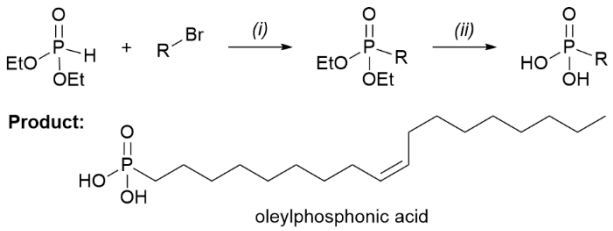

Scheme 2. Method to synthesize oleylphosphonic acid. Conditions: (i) 4h at 70 °C with NaH in dry DMF. (ii) 2.3 eq. of TMS-Br, overnight in dry DCM, then dry MeOH, 6h, 40 °C.

Synthesis of HfO_2, CdSe, and ZnS nanocrystal model systems. Hafnium oxide (HfO_2) NCs are synthesized via a surfactant-free solvothermal method; reacting hafnium *tert*-butoxide with benzyl alcohol (Figure 1A).[73] In the absence of ligands, the NCs are highly aggregated but upon addition of oleic acid, the NCs are stable in nonpolar solvents such as chloroform and benzene. The NCs are about 2.6 ± 0.3 nm ($\mu \pm \sigma$) in diameter according to transmission electron microscopy (TEM, Figure 1B). They are well purified, showing only broadened resonances in the ^{1}H NMR spectrum pertaining to bound oleate (Figure S1). Diffusion ordered NMR spectroscopy (DOSY) confirms the bound nature of the oleate since the oleate diffusion coefficient (89 $\mu m^2/s$) agrees with an object that has a solvodynamic diameter of 8.1 nm (Figure 1C and S1). This size is slightly larger than expected (around 6 nm), which could be due to some residual aggregation.

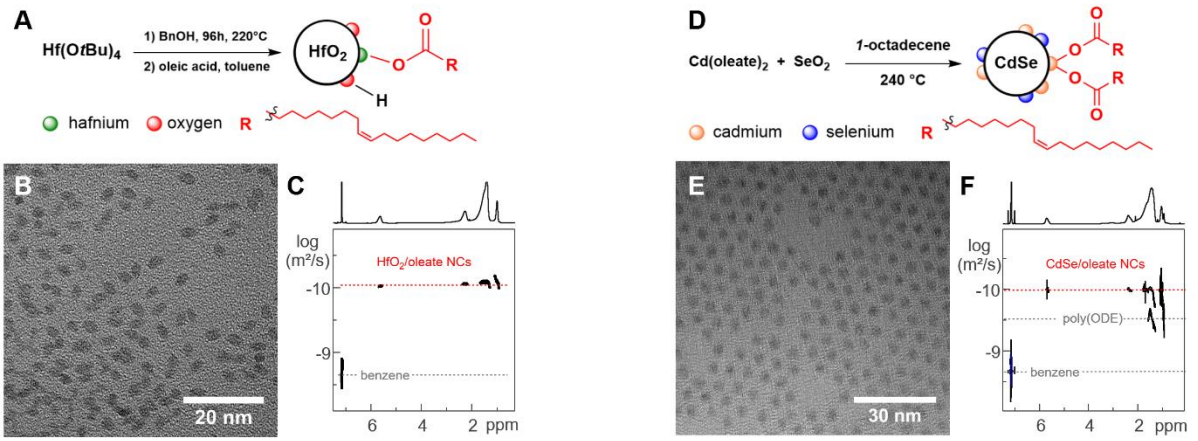

Figure 1. (A) General reaction scheme towards monoclinic HfO_2/oleate NCs, (B) TEM image, and (C) DOSY NMR spectrum in C_6D_6 of HfO_2(oleate) NCs. (D) General reaction scheme towards zinc blende CdSe/oleate NCs, (E) TEM image, and (F) DOSY NMR spectrum in C_6D_6 of CdSe/oleate NCs.

Cadmium selenide (CdSe) NCs capped with oleate ligands are synthesized by a reaction between cadmium oleate and selenium dioxide (SeO_2) (Figure 1D) reported by Chen *et al.*[74] The NCs have a diameter of about 4.1 ± 0.2 nm (μ ± σ) according to TEM (Figure 1E) and 4.1 nm according to UV-vis (Figure S2). Since the synthesis of these CdSe NCs requires *1*-octadecene (ODE), it is expected that a certain amount of poly(*1*-octadecene) is formed and not completely removed during purification, even with methyl acetate as a nonsolvent.[36] In the ^{1}H NMR spectrum, two sets of methyl (CH_3) peaks are indeed visible (Figure S2). Diffusion ordered NMR spectroscopy (DOSY) confirms the bound nature of the oleate since the oleate diffusion coefficient (97 $\mu m^2/s$) agrees with an object that has a solvodynamic diameter of 7.4 nm (Figure 1F and S2).

Zinc sulfide (ZnS) NCs (d = 2.6 nm) capped with oleate ligands are synthesized by a reaction between zinc oleate and *N,N,N'*-tribenzylthiourea (Figure S3).[75] The NCs were similarly characterized as the other model systems, see Figure S3.

Exchange of carboxylate for monoalkyl phosphinate. We have chosen oleate as the carboxylate in our model systems because it features the isolated alkene resonance around 5.5 ppm in the ^{1}H NMR spectrum (see Figure 2). As the incoming X-type ligand, we choose *6*-(hexyloxy)hexylphosphinic acid, featuring the CH_2-O-CH_2 resonances around 3.5 ppm, distinct from the alkene protons and from the aliphatic signals (Figure 2). We can thus quantify the amount of bound and free ligands in the following titrations. We perform the titrations in benzene-d_6 instead of chloroform-*d* due the larger chemical shift difference between free and bound ligands in benzene-d_6, improving the accuracy of the analysis.[60]

We gradually add the phosphinic acid to a dispersion of oleate capped HfO_2 or CdSe NCs (Figure 2A and 2E). During the titration, we observe for both systems that the broad alkene resonance (5.65 ppm, bound oleate) decreases in intensity (Figure 2B and 2F). A sharp alkene resonance (5.50 ppm) appears and increases in intensity throughout the titration. We assign the sharp alkene resonance to free oleic acid. In addition, a broad ether resonance (3.55 ppm) gradually increases in intensity, and corresponds to bound phosphinate. After addition of about one equivalent of phosphinic acid, the ^{31}P NMR spectrum contains a very broad resonance (fwhm = 2400 Hz), confirming the binding of phosphinate ligands to the NC surface (Figure 2C and 2G). When the titration is stopped here, and the NCs are purified (suspended in a minimal amount of benzene, and precipitated by addition of acetonitrile), we observe in the ^{1}H NMR spectrum of the supernatant the typical resonances of oleic acid (Figure S4 and S5), confirming the proton transfer during the X-for-X type exchange. The amounts of free and bound ligand over the course of the titration are plotted in Figure 2D and 2H. The amount of bound oleate decreases linearly (within error). The amount of free oleic acid and bound phosphinate are equal (within error), confirming the one-for-one nature of the exchange. No free phosphinic acid is detected in ^{1}H or ^{31}P NMR until the end of the titration. We conclude that the exchange of carboxylate for monoalkyl phosphinate goes to completion (i.e., an

irreversible reaction). Note that we do observe a small amount of free phosphinic acid, when 5 and 10 % of oleate is still bound for HfO_2 and CdSe respectively. The very last part of the exchange is thus slightly hindered.

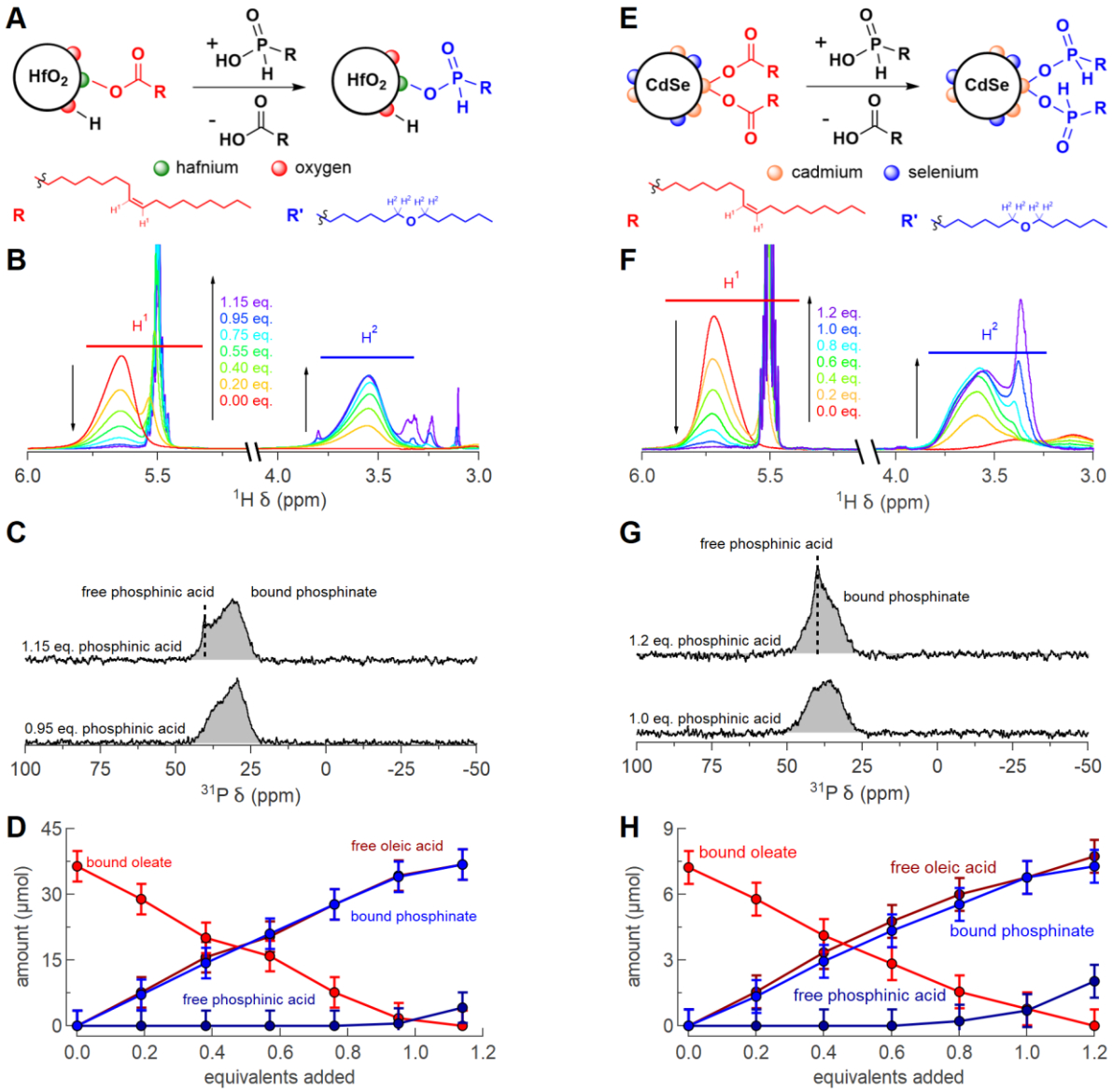

Figure 2. (left) Titration of HfO_2/oleate with 6-(hexyloxy)hexylphosphinic acid. (A) General reaction scheme, (B) ^{1}H NMR spectra of the titration, (C) ^{31}P NMR after 0.95 and 1.15 equivalent phosphinic acid is added, and (D) quantification of the different compounds as a function of added equivalents. (right) Titration of CdSe/oleate with 6-(hexyloxy)hexylphosphinic acid. (E) General reaction scheme,

(F) ^{1}H NMR spectra of the titration, (G) ^{31}P NMR after 1.0 and 1.2 equivalent phosphinic acid is added, and (H) quantification of the different compounds as a function of added equivalents.

We performed a similar titration with oleate capped ZnS NCs (Figure S6). Qualitatively, the same behaviour is observed as in Figure 2. Quantitatively, the bound oleate also decreases linearly but full exchange is not reached at 1 equivalent but at 1.6 equivalents of phosphinic acid. For the ether resonance, we observe a broad resonance (bound phosphinate) and a sharp resonance, even at the start of the titration. The sharp resonance is *not* assigned to free phosphinic acid since the ^{31}P NMR spectrum (Figure S6C) shows a sharp resonance at 34.5 ppm, inconsistent with free phosphinic acid (38.8 ppm). We identified the side-product as monoalkyl phosphinic acid anhydride, which shows the correct chemical shift in ^{31}P NMR. The anhydride was independently synthesized by dehydrating monoalkyl phosphinic anhydride with dicyclohexylcarbodiimide (DCC) (Figure S8). We thus infer that two parallel reactions are occurring: an irreversible X-for-X type exchange and a dehydration (catalysed by ZnS). The X-for-X type exchange is confirmed by the one-to-one correspondence of free oleic acid and bound phosphinate (Figure S6D). About one third of the added ligands reacts to form a side product. After addition of 1.6 equivalents phosphinic acid, the nanocrystals are precipitated by acetonitrile and isolated by centrifugation. In the ^{1}H NMR spectrum of the supernatant, we observe the characteristic resonances of oleic acid and also a set of resonances that are consistent with *6*-(hexyloxy)hexylphosphinic acid (Figure S7A). The identity of the latter is confirmed by the ^{31}P NMR spectrum featuring a resonance at 38.6 ppm (Figure S7B). Upon purification with polar solvents (containing water), the anhydride thus hydrolyses back to the phosphinic acid.

Exchange of monoalkyl phosphinate for phosphonate. Upon complete exchange of oleate for *6*-(hexyloxy)hexylphosphinate, the HfO_2 and CdSe NCs were purified by precipitation with acetonitrile. The purified NCs (Figure 3, S9 and S10) feature a broad ether resonance around

3.55 ppm and any free *6*-(hexyloxy)hexylphosphinic acid is absent (see also the ^{31}P NMR spectrum in the inset of Figure 3B). This is our starting point to analyse the X-type ligand exchange from phosphinate to phosphonate.

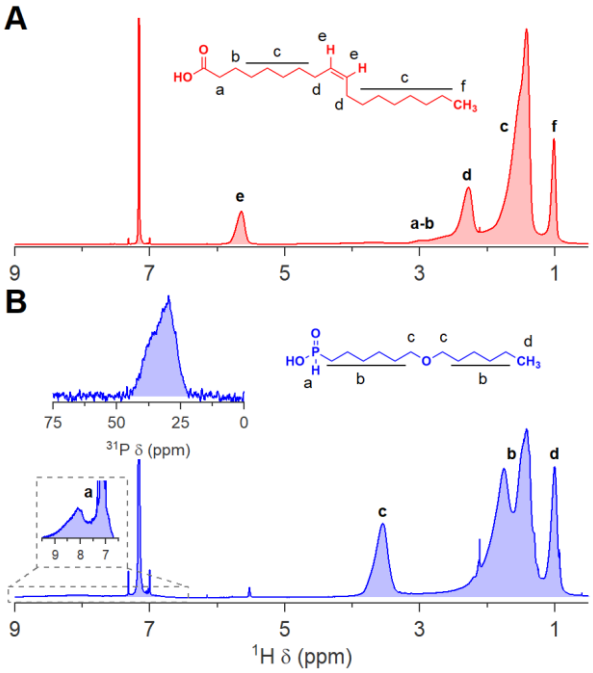

Figure 3. (A) ^{1}H NMR spectrum of oleate capped HfO_2 NCs in C_6D_6. (B) ^{1}H NMR spectrum of HfO_2 in C_6D_6, after ligand exchange for *6*-(hexyloxy)hexylphosphinic acid and purification. The inset shows the ^{31}P NMR spectrum.

Upon addition of oleylphosphonic acid to the nanocrystals (Figure 4), a broad alkene resonance appears (5.6 ppm), assigned to bound oleylphosphonate. The broad alkene resonance increases in intensity throughout the titration but a sharp alkene resonance is present as well. The latter corresponds to free phosphonic acid. During the titration, the bound phosphinate resonances decreases in intensity and a sharp resonance corresponding to free phosphinic acid appears. At two equivalents of phosphonic acid added, we observe both bound phosphonate and bound phosphinate. After purification of the nanocrystals, we retrieve the expected signals of both *6*-(hexyloxy)hexylphosphinic and oleylphosphonic acid in the ^{1}H and ^{31}P NMR spectra of the supernatant (Figure S13 and S14). It is interesting to look at the quantification of all free and

bound species during the titration (Figure 4C and 4F). The amount of free (released) phosphinic acid and the bound phosphonate are equal (within error) over the course of the titration, indicating again a one-for-one exchange. However, this time the reaction does not go to completion and the bound phosphinate saturates at 40 and 30 % for HfO_2 and CdSe respectively. Similar results are obtained for ZnS NCs, see Figures S11, S12, and S15. We conclude that the exchange is an equilibrium reaction.

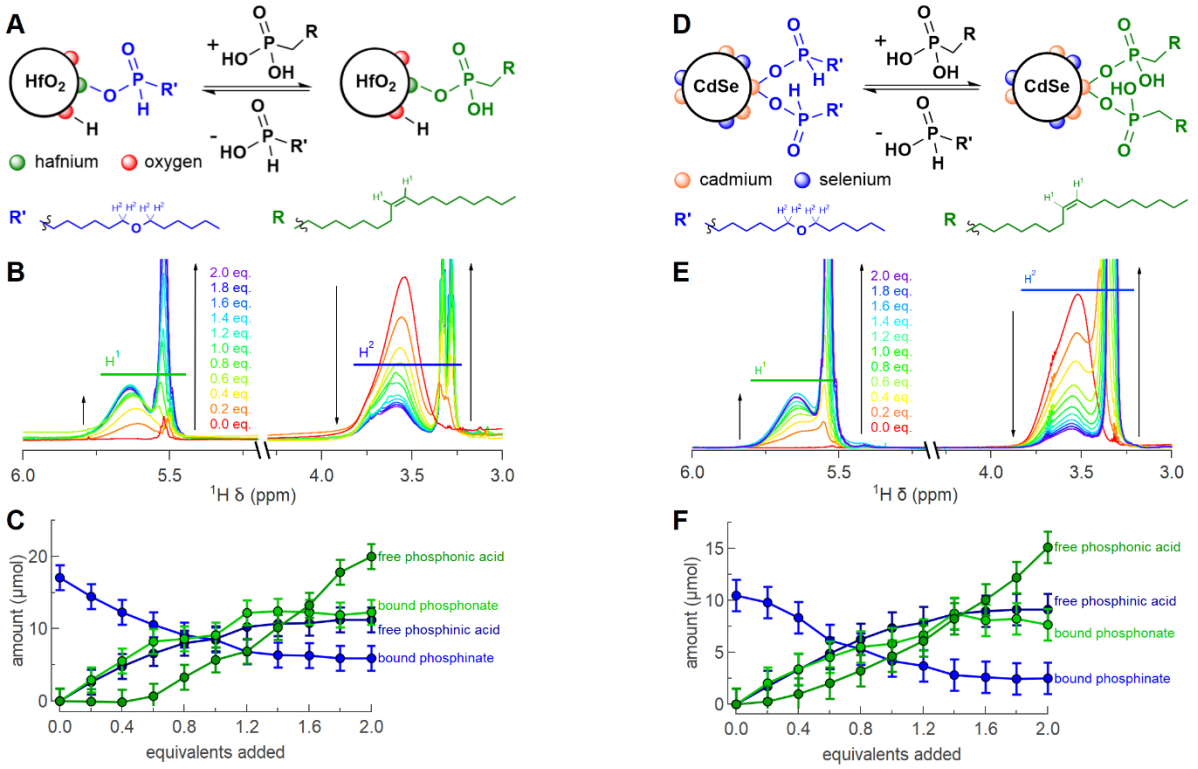

Figure 4. (left) Titration of HfO_2/[*6*-(hexyloxy)hexyl]phosphinate with oleylphosphonic acid. (A) General reaction scheme, (B) ^{1}H NMR spectra of the titration, and (C) quantification of the different compounds as a function of added equivalents. Note the small amount of residual oleic acid present at the start of the titration in panel B, due to a challenging purification (high solubility of the HfO_2/[*6*-(hexyloxy)hexyl]phosphinate NCs). This small signal was integrated and subtracted from the spectra for the quantification in panel C. (right) Titration of CdSe/[*6*-(hexyloxy)hexyl]phosphinate with oleylphosphonic acid. (D) General reaction scheme, (E) ^{1}H NMR spectra of the titration, and (F) quantification of the different compounds as a function of added equivalents.

The equilibrium can be schematically written as:

$$NC(phosphin) + phosphon\text{-}H \rightleftharpoons NC(phosphon) + phosphin\text{-}H \quad (1)$$

To gain quantitative insight in the equilibrium, we compare the composition of the ligand shell with the overall ligand composition in the mixture, as has been done before.[41, 76] The composition of the ligand shell is expressed by the mole fraction of phosphonate.

$$\chi_{phosphon\ (bound)} = \frac{n_{phosphonate\ (bound)}}{n_{phosphinate\ (bound)} + n_{phosphonate\ (bound)}} \quad (2)$$

The overall ligand composition is expressed as the mole fraction of phosphonate/phosphonic acid in the whole mixture, irrespective of the bound or free nature of the ligand.

$$\chi_{phosphon\ (total)} = \frac{n_{phosphon\ (total)}}{n_{phosphin\ (total)} + n_{phosphon\ (total)}} \quad (3)$$

If $\chi_{phosphon\ (bound)} = \chi_{phosphon\ (total)}$, the composition of the ligand is equal to the overall composition and the equilibrium constant, K = 1. If $\chi_{phosphon\ (bound)} > \chi_{phosphon\ (total)}$, the surface is enriched in phosphonate and K > 1. We can calculate both mole fractions since all components (free and bound species) are independently determined from the NMR spectra. In Figure 5, $\chi_{phosphon\ (bound)}$ is plotted as a function of $\chi_{phosphon\ (total)}$, for both titrations with HfO_2, CdSe, and ZnS. Figure 5 also contains equilibrium lines, which indicate the expected behaviour for a theoretical equilibrium constant (see Table S1 and Equations S1 – S5 for details on the calculation). While the data shows some scatter, it is clear that the equilibrium constant is between 1 and 5, and the data agrees best with K = 2. This translates in a small free energy change; ΔG = -1.7 kJ/mol.

To confirm the reversibility of the exchange, we purify the HfO_2, CdSe and ZnS NCs after the titration (Figure S16B, S17B, and S18B). Starting from the mixed ligand shell (with both *6*-

(hexyloxy)hexylphosphinate and oleylphosphonate bound to the surface), we push the equilibria back to bound phosphinate by adding *6*-(hexyloxy)hexylphosphinic acid (Figure S16C, S17C, and S18C). As expected, the bound phosphonate resonance decreases in intensity throughout the titration, and a sharp alkene resonance (free phosphonic acid) appears as well. We conclude that the X-type ligand exchange is reversible.

Discussion on accuracy of thermodynamic values. From Figure 5 it follows that the ligand exchange is reasonably well described by a single equilibrium constant (within error, K = 1 – 5). This stands in contrast to the desorption of Z-type cadmium oleate from CdSe NCs (where K could vary two orders of magnitude for different binding sites).[77] Given the comparative nature of the X-type ligand exchange, it is indeed not expected to observe big differences in K for different binding sites. Even the specific metal center (Hf, Cd, Zn) is quite unimportant since the observed equilibrium constant is the same for all NC systems studied (see Figure 5). For clarity, the traces are individually plotted in Figure S19.

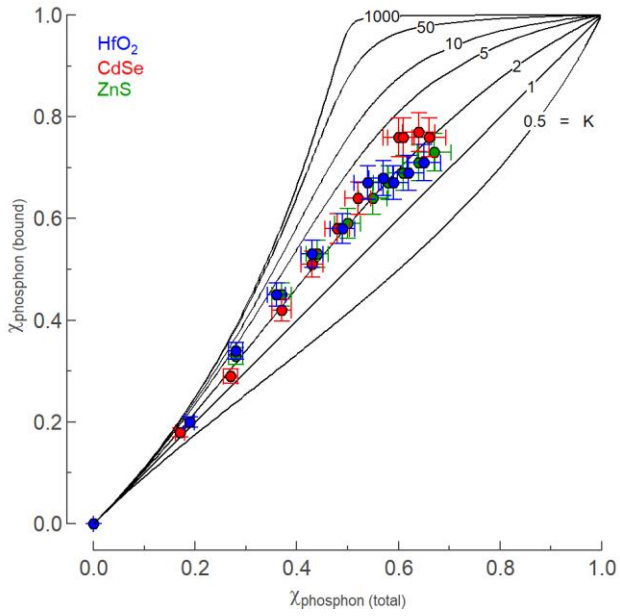

Figure 5. The mole fraction of bound oleylphosphonate in the ligand shell, $\chi_{phosphon\,(bound)}$, as a function of the overall mole fraction of oleylphosphonic acid (= unbound phosphonic acid and bound

phosphonate), $\chi_{phosphon\ (total)}$, during the titrations of HfO_2 (blue), CdSe (red), and ZnS (green) NCs. The full lines represent different calculated equilibrium constants.

When determining the equilibrium constant of an exchange reaction, we consider that the following aspects impact the accuracy. (1) At low equivalents of the incoming ligand, small errors in the determined mole fraction lead to large errors in equilibrium constants. This is graphically seen in the lower left corner of Figure 5 where all equilibrium lines are very close to one another. (2) Specific to the NMR spectroscopic technique, at low equivalents, the "free" ligand resonances are not well separated from the bound ligand resonances. It is well reported that free ligands can still interact with the ligand shell by Van der Waals interactions.[78] The higher the concentration of free ligands, or the higher the concentration of competing ligands, the better resolved the free resonance is, and the more accurately it can be integrated, see also Figure S20. For these reasons, it is not advised to do a "point calculation" of the reaction quotient at low mole fractions of the incoming ligand.

Conclusion

We have investigated the relative binding affinity of monoalkyl phosphinic acid ligands for HfO_2, CdSe, and ZnS NC surfaces in nonpolar environment. To monitor all species in an X-for-X-type ligand exchange in ^{1}H NMR, we synthesized *6*-(hexyloxy)hexylphosphinic and oleylphosphonic acid which have distinct and isolated resonances at around 3.5 ppm and 5.5 ppm respectively. We found that monoalkyl phosphinate ligands irreversible replace carboxylates on the NC surface. Phosphonic acids can subsequently replace bound phosphinate, but the reaction does not go to completion. An equilibrium is established with K = 2. Phosphinic acid ligands have thus an intermediate binding affinity between carboxylic acids and phosphonic acids for the model systems employed (under acidic conditions):

Carboxylic acid << monoalkyl phosphinic acid < phosphonic acid.

These results further pave the way for a more widespread use of monoalkyl phosphinic acids in nanocrystal synthesis and post-synthetic surface functionalization.

Experimental Section

General considerations. All manipulations are performed in air, unless otherwise indicated. All chemicals are used as received unless otherwise mentioned. Lithium aluminium hydride (95%), and potassium hydrogen sulfate (99%) were purchased from Acros. Calcium hydride (92%), and *n*-hexadecane (95%) were purchased from Alfa Aesar. Benzene (99.5%), cadmium oxide (99.998%), magnesium turnings (99.9%), magnesium sulfate (99.0%), and chloroform-d1 (99.8%D stabilized with Ag) were purchased from Carl Roth. Acetone (99%), acetonitrile (99.9%), celite, chloroform (99.5%), dichloromethane (99.8%), diethyl ether (99.5%), ethanol absolute (99.9%), ethyl acetate (99.5%), *n*-hexane (99%), hydrochloric acid (37%), isopropanol (99.9%), methanol (99%), silica gel (60A), sodium chloride (99.8%), sodium hydroxide (98.5%), sodium sulfate (99%) tetrahydrofuran (99.9%), toluene (99.9%), and trifluoroacetic acid (99%) were purchased from Chem-Lab. *1,2*-Dibromoethane (98%), *1,6*-dibromohexane (96%), *1*-hexanol (98%), *1*-octadecene (90%), anhydrous benzyl alcohol (99.8%), benzyl isothiocyanate (98%), bromotrimethylsilane (97%), dibenzylamine (97%), *N,N'*-dicyclohexylcarbodiimide (99%), diethyl chlorophosphite (95%), hafnium(IV) *tert*-butoxide (99.999%), oleic acid (90%), potassium hydroxide (90%), sodium hydride (60% dispersion in mineral oil), sodium hypophosphite monohydrate (99%), tetrabromomethane (99%), tetraglyme (99%), triethylamine (99%), and zinc oxide (99.999%) were purchased from Sigma-Aldrich. Trifluoroacetic anhydride (98%) was purchased from TCI. Benzene-d6 (99.5%D), dichloromethane-d2 (99.8%D), and methanol-d4 (99.8%D) were purchased from VWR.

When required, organic solvents are dried according to the procedure described by Williams *et al.*[79] making use of 20% m/v 3Å sieves for minimum 120 hours. Tetraglyme, and *n*-hexadecane, were purified as follows. Calcium hydride is added to the solvent and vacuum dried overnight while stirring. Afterwards, the solvent is vacuum distilled and collected in a Straus flask to introduce it in the glovebox where it is stored over molecular sieves.

Oleylphosphonic acid is synthesized according to De Roo *et al*. in a four-step reaction procedure starting from oleic acid, leading to a more isomeric pure end product which result in a white solid at room temperature instead of a viscous colourless liquid.[33] In the first step oleic acid is reduced to oleyl alcohol, according to the procedure of Sytniczuk *et al*.[37, 69]

Synthesis of *1*-bromo-*6*-(hexyloxy)hexane. *1*-Bromo-*6*-(hexyloxy)hexane is synthesized according to the procedure of Okada *et al.* with slight adaptations.[80] A 250 mL Schlenkflask is loaded with sodium hydride (1500.0 mg, 37.5 mmol, 1.5 eq.) and dry tetrahydrofuran (65 mL) to which *1*-hexanol (2554.3 mg, 3.140 mL, 25 mmol, 1.0 eq.) is added dropwise. The mixture is stirred overnight at room temperature. Afterwards, *1,6*-dibromohexane (9148.9, 5.770 mL, 37.5 mmol, 1.0 eq.) is dropwise and let to stir at room temperature overnight. Methanol (65 mL) is added to quench the reaction, and concentrated on the rotary evaporator. Afterwards, the product is extracted twice using dichloromethane (50 mL) and water (50 mL). The organic fractions are combined, dried with sodium sulfate, and concentrated on the rotary evaporator before the product is vacuum distilled to purity to obtain a colourless liquid (2.3 g, 35%). **^{1}H NMR** (400MHz, $CDCl_3$): δ 3.42-3.32 (m, 6H), 1.90-1.80 (m, 2H), 1.65-1.15 (m, 14H), 0.86 (t, *J* = 7.1 Hz, 3H). **^{13}C NMR** (100MHz, $CDCl_3$): δ 71.18, 70.79, 33.91, 32.77, 31.87, 29.81, 28.17, 27.44, 26.01, 25.57, 22.78, 14.19. **GC-MS** calc for $C_{12}H_{25}BrO$ [M] 264.11, found 264.

Synthesis of ethyl [*6*-(hexyloxy)hexyl]phosphinate ester. Ethyl [*6*-(hexyloxy)hexyl]phosphinate ester is synthetized according to the procedure used to synthesize

oleylphosphinate ester of Dhaene *et al.*[37], which was inspired by Jia *et al.*[66] A 50 mL Schlenkflask is loaded with activated magnesium (364.7 mg, 15 mmol, 2.0 eq.), dry tetrahydrofuran (15 mL), *1*-bromo-*6*-(hexyloxy)hexane (1989.3 mg, 7.5 mmol, 1.0 eq.) and *1,2*-dibromoethane (50 µL), and stirred overnight at room temperature. Following, a 100 mL Schlenkflask is brought into an argon filled glovebox and loaded with diethyl chlorophosphite (1174.1 mg, 1.080 mL, 7.5 mmol, 1 eq.) and dry tetrahydrofuran (15 mL), and transferred to a Schlenkline. The Grignard solution is added by means of a filtered Cannula transfer to the phosphite solution, and stirred at 50 °C overnight. After the reaction mixture is concentration at the rotary evaporator, concentrated (12M, 37%) HCl (1.5 mL) and H_2O (22.5 mL) is added and left to stir for 2 hours. Afterwards, the product is extracted using dichloromethane (37.5 mL) twice. The organic fractions are combined, dried with sodium sulfate, and concentrated on the rotary evaporator before the product is purified using silica chromatography with ethyl acetate to obtain a colourless liquid (0.3 g, 10 %). **^{1}H NMR** (400MHz, $CDCl_3$): δ 7.69 (s, *J* = 1.9 Hz, 0.5H), 6.38 (s, *J* = 1.9 Hz, 0.5H), 4.20-3.95 (m, 2H), 3.34 (t, *J* = 6.6 Hz, 4H), 1.80-1.65 (m, 2H), 1.65-1.45 (m, 6H), 1.45-1.15 (m, 13H), 0.84 (t, *J* = 7 Hz, 3H). **^{13}C NMR** (100MHz, $CDCl_3$): δ 71.11, 70.73, 62.38, 31.81, 30.37, 29.83, 29.57, 29.28, 28.33, 25.91, 22.72, 20.80, 16.39, 14.13. **^{31}P[1H] NMR** (160MHz, $CDCl_3$): δ 38.83 ppm. **LC-MS** (API-ES) calc for $C_{14}H_{32}O_3P$ $[M+H]^+$ 279.21, found 279.2.

Synthesis of *6*-(hexyloxy)hexylphosphinic acid. *6*-(Hexyloxy)hexylphosphinic acid is synthetized according to the procedure used to synthesize oleylphosphinic acid of Dhaene *et al.*[37] A 25 mL Schlenkflask is loaded with [*6*-(hexyloxy)hexyl]phosphinate ester (268.0 mg, 1.00 mmol, 1.00 eq.), dry dichloromethane (1 mL) and bromotrimethylsilane (176.1 mg, 151.8 µL, 1.15 mmol, 1.15 eq.), and left stirring overnight at room temperature. After the volatiles are evaporated using dynamic vacuum extensively, dry methanol (2.5 mL) is added and left to stir for 4 hours at 40 °C. Afterwards, the mixture is vacuum dried overnight at 40 °C to obtain

a colourless liquid (quantitative yield). **^{1}H NMR** (400MHz, $CDCl_3$): δ 12.00 (s, 1H), 7.77 (s, 0.5H), 6.40 (s, 0.5H), 3.35 (t, *J* = 6.8 Hz, 4H), 1.75 (quin, *J* = 7.6 Hz, 2H), 1.65-1.45 (m, 6H), 1.45-1.15 (m, 10H), 0.85 (t, *J* = 7.0 Hz, 3H). **^{13}C NMR** (100MHz, $CDCl_3$): δ 71.15, 70.77, 31.82, 30.39, 30.23, 29.81, 29.55, 25.98, 25.86, 22.75, 20.66, 14.17. **^{31}P[1H] NMR** (160MHz, $CDCl_3$): δ 38.76. **LC-MS** (API-ES) calc for $C_{12}H_{28}O_3P$ $[M+H]^+$ 251.18, found 251.2.

Synthesis of zinc oleate. $Zn(oleate)_2$ is synthesized from ZnO and trifluoroacetic anhydride according to the procedure described by Bennett *et al.*[36, 81] On a 45 mmol scale, a yield of 27.6 g, 98 % is obtained. **^{1}H NMR** (400MHz, $CDCl_3$): 5.40-5.20 (m, 2H), 2.33 (t, *J* = 7.6 Hz, 2H), 2.00 (quad, J = 2.9 Hz, 4H), 1.60 (t, *J* = 6.3 Hz, 2H), 1.40-1.10 (m, 20H), 0.86 (t, *J* = 7.1 Hz, 3H).

Synthesis of *N,N,N'*-tribenzylthiourea. *N,N,N'*-tribenzylthiourea is synthesized as reported by Dhaene *et al.*,[82] according to the procedure by Hendricks *et al*. with an additional recrystallization step.[75, 83] A 40 mL vial is loaded with benzylisothiocyanate (4476.6 mg, 3.8 mL, 30 mmol, 1 eq.) and toluene (5 mL). To this, a solution of dibenzylamine (5918.4 mg, 5.8 mL, 30 mmol, 1 eq.) in toluene (5mL) is added dropwise, and let to stir for 1 hour. Afterwards, the solvent is removed on the rotary evaporator, and the solid product is recrystallized in acetonitrile (30 mL) to obtain the purified thiourea in the form of white needles (15.6 g, 75 %). **^{1}H NMR** (400MHz, CD_2Cl_2): 7.40-7.15 (m, 13H), 7.10-6.95 (m, 2H), 5.83 (t, *J* = 4.7 Hz, 1H), 5.00 (s, 4H), 4.82 (d, *J* = 2.7 Hz, 2H). **^{13}C NMR** (100MHz, $CDCl_3$): 183.16, 137.79, 136.07, 129.17, 128.76, 128.03, 127.63, 127.60, 127.19, 54.39, 50.81. **LC-MS (ESI)** m/z calculated for $C_{22}H_{23}N_2S$ $[M+H]^+$ 347.16, found: 347.1.

Synthesis of HfO_2 nanocrystals. HfO_2 NCs are synthesized according to the procedure of Lauria *et al.*,[73] and stabilized with oleate ligands. In a nitrogen filled glovebox, 45.6 mL of a premade stock solution of hafnium(IV) *tert*-butoxide (5.00 g, 4.30 mL, 10.6 mmol, 1 eq.) and

anhydrous benzyl alcohol (92.01 g, 88.48 mL, 851 mmol, 80 eq.) is loaded in a 125 mL Parr bomb. The Parr bomb is taken out of the glovebox and heated in a muffle furnace at 220 °C for 96 hours. After it cooled down to room temperature, its contents are divided into 2 centrifuge tubes to which diethylether (19 mL/tube) is added and centrifuged (5000 rcf, 5'). This wash step is repeated 3 times. Afterwards, toluene (19 mL/tube) and oleic acid (706.2 mg 790 µL, 2.5 mmol) are added, sonicated for 30 minutes, and centrifuged (5000 rcf, 5') to eliminate agglomerates. The NC colloid is precipitated with acetone (40 mL), centrifuged, and redispersed in toluene (5 mL) three times. Finally, the NCs are vacuum dried to obtain a white powder.

Synthesis of CdSe nanocrystals. CdSe NCs are synthesized according to Chen *et al*.[74] When the desired size is reached (3.3 nm), the reaction is quenched with a tenfold excess of oleic acid, resulting in oleate capped NCs. The CdSe NCs were purified 3 times with methyl acetate/THF as non-solvent/solvent combination. Finally, the NCs are vacuum dried to obtain a sticky, orange powder.

Synthesis of ZnS nanocrystals. ZnS NCs are synthesized similar to the procedure used to synthesize lead sulfide (PbS) NCs of Hendricks *et al*. with some slight modifications.[75] The original solvent (*1*-octadecene) has been replace by *n*-hexadecane to prevent polymerization during synthesis and contamination in the final product.[36] In an argon filled glovebox, a 25 mL three neck flask is loaded with zinc oleate (188.5 mg, 0.30 mmol, 1.2 eq.) and *n*-hexadecane (7.3435 g, 9.5 mL), and separately a 4 mL vial with *N,N,N'*-tribenzylthiourea (69.2 mg, 0.2 mmol, 1.0 eq.) is dissolved in tetraglyme (504.5 mg, 0.5 mL). The three neck flask is transferred to the Schlenkline and heated to 240 °C prior to the injection of the thiourea solution. After 2 hours at 240 °C, the reaction mixture is allowed to cool down to room temperature. After synthesis, the NCs are collected by adding acetone (40 mL) as nonsolvent to the reaction mixture and subsequent centrifugation (10 min, 10k rpm). The precipitate is redispersed in

toluene (5 mL) and pushed through a syringe filter with a pore size of 200 nm to remove the excess insoluble zinc oleate. The NC colloid is precipitated with acetone (40 mL), centrifuged, and redispersed in toluene (5 mL) three times. Finally, the NCs are vacuum dried to obtain a white powder.

Transmission electron microscopy. TEM and High-Resolution TEM were performed on a JEOL JEM-2200FS TEM with Cs corrector operated at 200 kV, and a JEOL JEM2800 field emission gun microscope operated at 200 kV equipped with a TVIPS XF416ES TEM camera.

NMR spectroscopy. Nuclear Magnetic Resonance (NMR) spectra of the synthesized organics were recorded on a Bruker 300, and 400 MHz. Chemical shifts (δ) are given in ppm and the residual solvent peak was used as an internal standard ($CDCl_3$: δH = 7.24 ppm, δC = 77.06 ppm, CD_2Cl_2: δH = 5.32 ppm, δC = 53.84 ppm, C_6D_6: δH = 7.16 ppm, δC = 128.06 ppm). The signal multiplicity is denoted as follows: s (singlet), d (doublet), t (triplet), quad (quadruplet), quin (quintet), m (multiplet). Coupling constants are reported in Hertz (Hz). ^{1}H, ^{13}C, and ^{31}P spectra were acquired using the standard pulse sequences from the Bruker library; zg30, jmod (Attached Proton Test = APT), and zgpg30 (proton decoupled) respectively. In the APT, the carbon resonances resulting from a $-CH_2-$ and quaternary −Cq– are "in-phase" (orientated up), whereas the carbon resonances resulting from a $-CH_3-$ or −CH– are "out-of-phase" (orientated down), although one could easily reverse the phase 180° and achieve the inverse result. ^{31}P spectra of organic compounds were acquired with proton decoupling (zgpg30) and a relaxation delay (recycle delay, or D1) of 2 s. All resonances were corrected prior to integration by subtracting a background from the measured intensity. The chemical shifts for other nuclei were referenced indirectly to the ^{1}H NMR frequency of the sample with the "xiref"-macro in Bruker.

Nuclear Magnetic Resonance (NMR) measurements of colloidal nanocrystals were recorded on a Bruker Avance III Spectrometer operating at a ^{1}H frequency of 500.13 MHz and featuring a

BBI probe, and on a Bruker Avance III Spectrometer operating at a ^{1}H frequency of 600.13 MHz. The sample temperature was set to 298.15 K. For the quantitative 1D ^{1}H measurements, 64k data points were sampled with the spectral width set to 16 ppm and a relaxation delay of 30 s to allow full relaxation of all NMR signals. The quantification was done by using the Digital ERETIC method.[84, 85] One-dimensional ^{31}P spectra were acquired using the standard pulse sequence zggpseig from the Bruker library [with a tau echo delay, i.e., D16 = 200 μs, and a relaxation delay (D1) of 2 s]. DOSY measurements were performed with a double stimulated echo pulses (dstegp3s) for convection compensation and with monopolar gradient pulses,[86] and a relaxation delay (D1) of 1 s. The gradient strength was varied quadratically from 2-95% of the probe's maximum value in 64 steps, with the pulse length gradient (D20) and diffusion time (P30) optimized to ensure a final attenuation of the signal in the final increment of less than 10% relative to the first increment.

Mass spectroscopy. Mass spectra (MS) are measured with an Agilent ESI single quadrupole detector type VL and an Agilent APCI single quadrupole detector type VL.

Size determination. The optical band gaps of the NCs were determined by UV–vis–NIR absorption spectroscopy (PerkinElmer Lambda 365 and PerkinElmer Lambda 950). The size of the CdSe and ZnS NCs was determined from the position of the first excitonic absorption peak using the sizing curve described by Maes *et al*.[87] and Bennett *et al*.[81] respectively.

Acknowledgements

The authors acknowledge the FWO Vlaanderen (FWO-SB grant 1S28820N and 1SA4221N), Special Research Fund/Concerted Research Actions project (BOF2015/GOA/007), Ghent

University, and University of Basel for financial support. The authors thank ing. Jan Goeman for the GC/LC-MS.

Associated Content

Supporting information

Additional ^{1}H, ^{31}P, and DOSY NMR spectra, TEM images, UV-Vis spectra, additional ligand exchange reactions and titrations, tables with calculated equilibrium constants, equilibrium constant calculations, and NMR spectra of synthesized compounds.

References

1. Baek, W.; Chang, H.; Bootharaju, M. S.; Kim, J. H.; Park, S.; Hyeon, T., Recent Advances and Prospects in Colloidal Nanomaterials. *JACS Au* **2021,** 1, (11), 1849-1859.
2. Zito, J.; Infante, I., The Future of Ligand Engineering in Colloidal Semiconductor Nanocrystals. *Accounts of Chemical Research* **2021,** 54, (7), 1555-1564.
3. Owen, J., The coordination chemistry of nanocrystal surfaces. *Science* **2015,** 347, (6222), 615-616.
4. De Roo, J.; De Keukeleere, K.; Hens, Z.; Van Driessche, I., From ligands to binding motifs and beyond; the enhanced versatility of nanocrystal surfaces. *Dalton Transactions* **2016,** 45, (34), 13277-13283.
5. Boles, M. A.; Ling, D.; Hyeon, T.; Talapin, D. V., The surface science of nanocrystals. *Nature Materials* **2016,** 15, (2), 141-153.
6. Calvin, J. J.; Brewer, A. S.; Alivisatos, A. P., The role of organic ligand shell structures in colloidal nanocrystal synthesis. *Nature Synthesis* **2022,** 1, (2), 127-137.
7. Doblas, D.; Kister, T.; Cano-Bonilla, M.; González-García, L.; Kraus, T., Colloidal Solubility and Agglomeration of Apolar Nanoparticles in Different Solvents. *Nano Letters* **2019,** 19, (8), 5246-5252.
8. Anderson, N. C.; Hendricks, M. P.; Choi, J. J.; Owen, J. S., Ligand Exchange and the Stoichiometry of Metal Chalcogenide Nanocrystals: Spectroscopic Observation of Facile Metal-Carboxylate Displacement and Binding. *Journal of the American Chemical Society* **2013,** 135, (49), 18536-18548.
9. Kirkwood, N.; Monchen, J. O. V.; Crisp, R. W.; Grimaldi, G.; Bergstein, H. A. C.; du Fossé, I.; van der Stam, W.; Infante, I.; Houtepen, A. J., Finding and Fixing Traps in II–VI and III–V Colloidal Quantum Dots: The Importance of Z-Type Ligand Passivation. *Journal of the American Chemical Society* **2018,** 140, (46), 15712-15723.
10. Giansante, C.; Infante, I., Surface Traps in Colloidal Quantum Dots: A Combined Experimental and Theoretical Perspective. *The Journal of Physical Chemistry Letters* **2017,** 8, (20), 5209-5215.

11. Houtepen, A. J.; Hens, Z.; Owen, J. S.; Infante, I., On the Origin of Surface Traps in Colloidal II–VI Semiconductor Nanocrystals. *Chemistry of Materials* **2017,** 29, (2), 752-761.
12. Wang, W.; Zhang, M.; Pan, Z.; Biesold, G. M.; Liang, S.; Rao, H.; Lin, Z.; Zhong, X., Colloidal Inorganic Ligand-Capped Nanocrystals: Fundamentals, Status, and Insights into Advanced Functional Nanodevices. *Chemical Reviews* **2022,** 122, (3), 4091-4162.
13. Kovalenko, M. V.; Scheele, M.; Talapin, D. V., Colloidal Nanocrystals with Molecular Metal Chalcogenide Surface Ligands. *Science* **2009,** 324, (5933), 1417-1420.
14. Green, M. L. H.; Parkin, G., Application of the Covalent Bond Classification Method for the Teaching of Inorganic Chemistry. *Journal of Chemical Education* **2014,** 91, (6), 807-816.
15. De Roo, J.; Justo, Y.; De Keukeleere, K.; Van den Broeck, F.; Martins, J. C.; Van Driessche, I.; Hens, Z., Carboxylic-Acid-Passivated Metal Oxide Nanocrystals: Ligand Exchange Characteristics of a New Binding Motif. *Angewandte Chemie International Edition* **2015,** 54, (22), 6488-6491.
16. Deblock, L.; Goossens, E.; Pokratath, R.; De Buysser, K.; De Roo, J., Mapping out the Aqueous Surface Chemistry of Metal Oxide Nanocrystals: Carboxylate, Phosphonate, and Catecholate Ligands. *JACS Au* **2022,** 2, (3), 711-722.
17. Chen, P. E.; Anderson, N. C.; Norman, Z. M.; Owen, J. S., Tight Binding of Carboxylate, Phosphonate, and Carbamate Anions to Stoichiometric CdSe Nanocrystals. *Journal of the American Chemical Society* **2017,** 139, (8), 3227-3236.
18. Moreels, I.; Justo, Y.; De Geyter, B.; Haustraete, K.; Martins, J. C.; Hens, Z., Size-Tunable, Bright, and Stable PbS Quantum Dots: A Surface Chemistry Study. *ACS Nano* **2011,** 5, (3), 2004-2012.
19. De Roo, J.; Van Driessche, I.; Martins, J. C.; Hens, Z., Colloidal metal oxide nanocrystal catalysis by sustained chemically driven ligand displacement. *Nature Materials* **2016,** 15, (5), 517-521.
20. Knauf, R. R.; Lennox, J. C.; Dempsey, J. L., Quantifying Ligand Exchange Reactions at CdSe Nanocrystal Surfaces. *Chemistry of Materials* **2016,** 28, (13), 4762-4770.
21. Ritchhart, A.; Cossairt, B. M., Quantifying Ligand Exchange on InP Using an Atomically Precise Cluster Platform. *Inorganic Chemistry* **2019,** 58, (4), 2840-2847.
22. Calvin, J. J.; O'Brien, E. A.; Sedlak, A. B.; Balan, A. D.; Alivisatos, A. P., Thermodynamics of Composition Dependent Ligand Exchange on the Surfaces of Colloidal Indium Phosphide Quantum Dots. *ACS Nano* **2021,** 15, (1), 1407-1420.
23. De Keukeleere, K.; Coucke, S.; De Canck, E.; Van Der Voort, P.; Delpech, F.; Coppel, Y.; Hens, Z.; Van Driessche, I.; Owen, J. S.; De Roo, J., Stabilization of Colloidal Ti, Zr, and Hf Oxide Nanocrystals by Protonated Tri-n-octylphosphine Oxide (TOPO) and Its Decomposition Products. *Chemistry of Materials* **2017,** 29, (23), 10233-10242.
24. Hartley, C. L.; Kessler, M. L.; Dones Lassalle, C. Y.; Camp, A. M.; Dempsey, J. L., Effects of Ligand Shell Composition on Surface Reduction in PbS Quantum Dots. *Chemistry of Materials* **2021,** 33, (22), 8612-8622.
25. Kessler, M. L.; Starr, H. E.; Knauf, R. R.; Rountree, K. J.; Dempsey, J. L., Exchange equilibria of carboxylate-terminated ligands at PbS nanocrystal surfaces. *Physical Chemistry Chemical Physics* **2018,** 20, (36), 23649-23655.
26. Green, P. B.; Yarur Villanueva, F.; Imperiale, C. J.; Hasham, M.; Demmans, K. Z.; Burns, D. C.; Wilson, M. W. B., Directed Ligand Exchange on the Surface of PbS Nanocrystals: Implications for Incoherent Photon Conversion. *ACS Applied Nano Materials* **2021,** 4, (6), 5655-5664.
27. Karpov, O. N.; Bondarenko, G. N.; Merekalov, A. S.; Shandryuk, G. A.; Zhigalina, O. M.; Khmelenin, D. N.; Skryleva, E. A.; Golovan, L. A.; Talroze, R. V., Formation of the Inorganic and Organic Shells on the Surface of CdSe Quantum Dots. *ACS Applied Materials & Interfaces* **2021,** 13, (30), 36190-36200.
28. Yamashita, S.; Sudo, T.; Kamiya, H.; Okada, Y., Ligand Exchange Reactions between Phosphonic Acids at TiO2 Nanoparticle Surfaces. *ChemistrySelect* **2021,** 6, (12), 2923-2927.
29. Smock, S. R.; Williams, T. J.; Brutchey, R. L., Quantifying the Thermodynamics of Ligand Binding to CsPbBr3 Quantum Dots. *Angewandte Chemie International Edition* **2018,** 57, (36), 11711-11715.

30. De Roo, J.; Van den Broeck, F.; De Keukeleere, K.; Martins, J. C.; Van Driessche, I.; Hens, Z., Unravelling the Surface Chemistry of Metal Oxide Nanocrystals, the Role of Acids and Bases. *Journal of the American Chemical Society* **2014,** 136, (27), 9650-9657.
31. Gomes, R.; Hassinen, A.; Szczygiel, A.; Zhao, Q.; Vantomme, A.; Martins, J. C.; Hens, Z., Binding of Phosphonic Acids to CdSe Quantum Dots: A Solution NMR Study. *The Journal of Physical Chemistry Letters* **2011,** 2, (3), 145-152.
32. Gee, M. Y.; Shen, Y.; Greytak, A. B., Isothermal Titration Calorimetry Resolves Sequential Ligand Exchange and Association Reactions in Treatment of Oleate-Capped CdSe Quantum Dots with Alkylphosphonic Acid. *The Journal of Physical Chemistry C* **2020,** 124, (43), 23964-23975.
33. De Roo, J.; Zhou, Z.; Wang, J.; Deblock, L.; Crosby, A. J.; Owen, J. S.; Nonnenmann, S. S., Synthesis of Phosphonic Acid Ligands for Nanocrystal Surface Functionalization and Solution Processed Memristors. *Chemistry of Materials* **2018,** 30, (21), 8034-8039.
34. Jeong, D.-W.; Park, T.-H.; Lee, J. H.; Jang, D.-J., Efficient Addition of Desired Carboxylate Ligands to CdSe Quantum Dots Passivated with Phosphonic Acids. *The Journal of Physical Chemistry C* **2021,** 125, (41), 22929-22936.
35. Balan, A. D.; Olshansky, J. H.; Horowitz, Y.; Han, H.-L.; O'Brien, E. A.; Tang, L.; Somorjai, G. A.; Alivisatos, A. P., Unsaturated Ligands Seed an Order to Disorder Transition in Mixed Ligand Shells of CdSe/CdS Quantum Dots. *ACS Nano* **2019,** 13, (12), 13784-13796.
36. Dhaene, E.; Billet, J.; Bennett, E.; Van Driessche, I.; De Roo, J., The Trouble with ODE: Polymerization during Nanocrystal Synthesis. *Nano Letters* **2019,** 19, (10), 7411-7417.
37. Dhaene, E.; Pokratath, R.; Aalling-Frederiksen, O.; Jensen, K. M. Ø.; Smet, P. F.; De Buysser, K.; De Roo, J., Monoalkyl Phosphinic Acids as Ligands in Nanocrystal Synthesis. *ACS Nano* **2022,** 16, (5), 7361-7372.
38. Calcabrini, M.; Van den Eynden, D.; Ribot, S. S.; Pokratath, R.; Llorca, J.; De Roo, J.; Ibáñez, M., Ligand Conversion in Nanocrystal Synthesis: The Oxidation of Alkylamines to Fatty Acids by Nitrate. *JACS Au* **2021,** 1, (11), 1898-1903.
39. Ibáñez, M.; Korkosz, R. J.; Luo, Z.; Riba, P.; Cadavid, D.; Ortega, S.; Cabot, A.; Kanatzidis, M. G., Electron Doping in Bottom-Up Engineered Thermoelectric Nanomaterials through HCl-Mediated Ligand Displacement. *Journal of the American Chemical Society* **2015,** 137, (12), 4046-4049.
40. Leemans, J.; Dümbgen, K. C.; Minjauw, M. M.; Zhao, Q.; Vantomme, A.; Infante, I.; Detavernier, C.; Hens, Z., Acid–Base Mediated Ligand Exchange on Near-Infrared Absorbing, Indium-Based III–V Colloidal Quantum Dots. *Journal of the American Chemical Society* **2021,** 143, (11), 4290-4301.
41. De Nolf, K.; Cosseddu, S. M.; Jasieniak, J. J.; Drijvers, E.; Martins, J. C.; Infante, I.; Hens, Z., Binding and Packing in Two-Component Colloidal Quantum Dot Ligand Shells: Linear versus Branched Carboxylates. *Journal of the American Chemical Society* **2017,** 139, (9), 3456-3464.
42. De Roo, J.; Huang, Z.; Schuster, N. J.; Hamachi, L. S.; Congreve, D. N.; Xu, Z.; Xia, P.; Fishman, D. A.; Lian, T.; Owen, J. S.; Tang, M. L., Anthracene Diphosphate Ligands for CdSe Quantum Dots; Molecular Design for Efficient Upconversion. *Chemistry of Materials* **2020,** 32, (4), 1461-1466.
43. Nemat, S. J.; Van den Eynden, D.; Deblock, L.; Heilmann, M.; Köster, J. M.; Parvizian, M.; Tiefenbacher, K.; De Roo, J., Resorcin[4]arene-based multidentate phosphate ligands with superior binding affinity for nanocrystal surfaces. *Chemical Communications* **2021,** 57, (38), 4694-4697.
44. Wang, W.; Mattoussi, H., Engineering the Bio–Nano Interface Using a Multifunctional Coordinating Polymer Coating. *Accounts of Chemical Research* **2020,** 53, (6), 1124-1138.
45. Elimelech, O.; Aviv, O.; Oded, M.; Banin, U., A Tale of Tails: Thermodynamics of CdSe Nanocrystal Surface Ligand Exchange. *Nano Letters* **2020,** 20, (9), 6396-6403.
46. Perez, K. A.; Lian, S.; Kodaimati, M. S.; He, C.; Weiss, E. A., Mechanisms of Defect Passivation by Fluorinated Alkylthiolates on PbS Quantum Dots. *The Journal of Physical Chemistry C* **2018,** 122, (25), 13911-13919.
47. Wei, N.; Li, L.; Zhang, H.; Wang, W.; Pan, C.; Qi, S.; Zhang, H.; Chen, H.; Chen, X., Characterization of the Ligand Exchange Reactions on CdSe/ZnS QDs by Capillary Electrophoresis. *Langmuir* **2019,** 35, (14), 4806-4812.

48. Grigel, V.; Sagar, L. K.; De Nolf, K.; Zhao, Q.; Vantomme, A.; De Roo, J.; Infante, I.; Hens, Z., The Surface Chemistry of Colloidal HgSe Nanocrystals, toward Stoichiometric Quantum Dots by Design. *Chemistry of Materials* **2018,** 30, (21), 7637-7647.
49. Kessler, M. L.; Kelm, J. E.; Starr, H. E.; Cook, E. N.; Miller, J. D.; Rivera, N. A.; Hsu-Kim, H.; Dempsey, J. L., Unraveling Changes to PbS Nanocrystal Surfaces Induced by Thiols. *Chemistry of Materials* **2022,** 34, (4), 1710-1721.
50. Owen, J. S.; Park, J.; Trudeau, P.-E.; Alivisatos, A. P., Reaction Chemistry and Ligand Exchange at Cadmium−Selenide Nanocrystal Surfaces. *Journal of the American Chemical Society* **2008,** 130, (37), 12279-12281.
51. Zhang, B.; Goldoni, L.; Lambruschini, C.; Moni, L.; Imran, M.; Pianetti, A.; Pinchetti, V.; Brovelli, S.; De Trizio, L.; Manna, L., Stable and Size Tunable CsPbBr3 Nanocrystals Synthesized with Oleylphosphonic Acid. *Nano Letters* **2020,** 20, (12), 8847-8853.
52. Zhang, B.; Goldoni, L.; Zito, J.; Dang, Z.; Almeida, G.; Zaccaria, F.; de Wit, J.; Infante, I.; De Trizio, L.; Manna, L., Alkyl Phosphonic Acids Deliver CsPbBr3 Nanocrystals with High Photoluminescence Quantum Yield and Truncated Octahedron Shape. *Chemistry of Materials* **2019,** 31, (21), 9140-9147.
53. Anderson, N. C.; Owen, J. S., Soluble, Chloride-Terminated CdSe Nanocrystals: Ligand Exchange Monitored by 1H and 31P NMR Spectroscopy. *Chemistry of Materials* **2013,** 25, (1), 69-76.
54. Caldwell, M. A.; Albers, A. E.; Levy, S. C.; Pick, T. E.; Cohen, B. E.; Helms, B. A.; Milliron, D. J., Driving oxygen coordinated ligand exchange at nanocrystal surfaces using trialkylsilylated chalcogenides. *Chemical Communications* **2011,** 47, (1), 556-558.
55. Pike, S. D.; White, E. R.; Shaffer, M. S. P.; Williams, C. K., Simple phosphinate ligands access zinc clusters identified in the synthesis of zinc oxide nanoparticles. *Nature Communications* **2016,** 7, (1), 13008.
56. Jasieniak, J.; Bullen, C.; van Embden, J.; Mulvaney, P., Phosphine-Free Synthesis of CdSe Nanocrystals. *The Journal of Physical Chemistry B* **2005,** 109, (44), 20665-20668.
57. van Embden, J.; Mulvaney, P., Nucleation and Growth of CdSe Nanocrystals in a Binary Ligand System. *Langmuir* **2005,** 21, (22), 10226-10233.
58. Shynkarenko, Y.; Bodnarchuk, M. I.; Bernasconi, C.; Berezovska, Y.; Verteletskyi, V.; Ochsenbein, S. T.; Kovalenko, M. V., Direct Synthesis of Quaternary Alkylammonium-Capped Perovskite Nanocrystals for Efficient Blue and Green Light-Emitting Diodes. *ACS Energy Letters* **2019,** 4, (11), 2703-2711.
59. Guo, Y.; Marchuk, K.; Sampat, S.; Abraham, R.; Fang, N.; Malko, A. V.; Vela, J., Unique Challenges Accompany Thick-Shell CdSe/nCdS (n > 10) Nanocrystal Synthesis. *The Journal of Physical Chemistry C* **2012,** 116, (4), 2791-2800.
60. De Roo, J.; Yazdani, N.; Drijvers, E.; Lauria, A.; Maes, J.; Owen, J. S.; Van Driessche, I.; Niederberger, M.; Wood, V.; Martins, J. C.; Infante, I.; Hens, Z., Probing Solvent–Ligand Interactions in Colloidal Nanocrystals by the NMR Line Broadening. *Chemistry of Materials* **2018,** 30, (15), 5485-5492.
61. Hens, Z.; Martins, J. C., A Solution NMR Toolbox for Characterizing the Surface Chemistry of Colloidal Nanocrystals. *Chemistry of Materials* **2013,** 25, (8), 1211-1221.
62. Abiodun, S. L.; Pellechia, P. J.; Greytak, A. B., Effective Purification of CsPbBr3 Nanocrystals with High Quantum Yield and High Colloidal Stability via Gel Permeation Chromatography. *The Journal of Physical Chemistry C* **2021,** 125, (6), 3463-3471.
63. Calvin, J. J.; Swabeck, J. K.; Sedlak, A. B.; Kim, Y.; Jang, E.; Alivisatos, A. P., Thermodynamic Investigation of Increased Luminescence in Indium Phosphide Quantum Dots by Treatment with Metal Halide Salts. *Journal of the American Chemical Society* **2020,** 142, (44), 18897-18906.
64. Edmundson, R. S., Properties and Reactions of Phosphonic and Phosphinic Acids and their Derivatives. In *PATAI'S Chemistry of Functional Groups*.
65. Deprèle, S.; Montchamp, J.-L., Triethylborane-Initiated Room Temperature Radical Addition of Hypophosphites to Olefins: Synthesis of Monosubstituted Phosphinic Acids and Esters. *The Journal of Organic Chemistry* **2001,** 66, (20), 6745-6755.

66. Jia, X.; Weber, S.; Schols, D.; Meier, C., Membrane Permeable, Bioreversibly Modified Prodrugs of Nucleoside Diphosphate-γ-Phosphonates. *Journal of Medicinal Chemistry* **2020,** 63, (20), 11990-12007.
67. Oliva-Puigdomènech, A.; De Roo, J.; Kuhs, J.; Detavernier, C.; Martins, J. C.; Hens, Z., Ligand Binding to Copper Nanocrystals: Amines and Carboxylic Acids and the Role of Surface Oxides. *Chemistry of Materials* **2019,** 31, (6), 2058-2067.
68. Loiudice, A.; Segura Lecina, O.; Bornet, A.; Luther, J. M.; Buonsanti, R., Ligand Locking on Quantum Dot Surfaces via a Mild Reactive Surface Treatment. *Journal of the American Chemical Society* **2021,** 143, (33), 13418-13427.
69. Sytniczuk, A.; Dąbrowski, M.; Banach, Ł.; Urban, M.; Czarnocka-Śniadała, S.; Milewski, M.; Kajetanowicz, A.; Grela, K., At Long Last: Olefin Metathesis Macrocyclization at High Concentration. *Journal of the American Chemical Society* **2018,** 140, (28), 8895-8901.
70. Appel, R., Tertiary Phosphane/Tetrachloromethane, a Versatile Reagent for Chlorination, Dehydration, and P-N Linkage. *Angewandte Chemie International Edition in English* **1975,** 14, (12), 801-811.
71. André, V.; Lahrache, H.; Robin, S.; Rousseau, G., Reaction of unsaturated phosphonate monoesters with bromo- and iodo(bis-collidine) hexafluorophosphates. *Tetrahedron* **2007,** 63, (40), 10059-10066.
72. McKenna, C. E.; Higa, M. T.; Cheung, N. H.; McKenna, M.-C., The facile dealkylation of phosphonic acid dialkyl esters by bromotrimethylsilane. *Tetrahedron Letters* **1977,** 18, (2), 155-158.
73. Lauria, A.; Villa, I.; Fasoli, M.; Niederberger, M.; Vedda, A., Multifunctional Role of Rare Earth Doping in Optical Materials: Nonaqueous Sol–Gel Synthesis of Stabilized Cubic HfO2 Luminescent Nanoparticles. *ACS Nano* **2013,** 7, (8), 7041-7052.
74. Chen, O.; Chen, X.; Yang, Y.; Lynch, J.; Wu, H.; Zhuang, J.; Cao, Y. C., Synthesis of Metal–Selenide Nanocrystals Using Selenium Dioxide as the Selenium Precursor. *Angewandte Chemie International Edition* **2008,** 47, (45), 8638-8641.
75. Hendricks, M. P.; Campos, M. P.; Cleveland, G. T.; Jen-La Plante, I.; Owen, J. S., A tunable library of substituted thiourea precursors to metal sulfide nanocrystals. *Science* **2015,** 348, (6240), 1226-1230.
76. Goldmann, C.; Ribot, F.; Peiretti, L. F.; Quaino, P.; Tielens, F.; Sanchez, C.; Chanéac, C.; Portehault, D., Quantified Binding Scale of Competing Ligands at the Surface of Gold Nanoparticles: The Role of Entropy and Intermolecular Forces. *Small* **2017,** 13, (20), 1604028.
77. Drijvers, E.; De Roo, J.; Martins, J. C.; Infante, I.; Hens, Z., Ligand Displacement Exposes Binding Site Heterogeneity on CdSe Nanocrystal Surfaces. *Chemistry of Materials* **2018,** 30, (3), 1178-1186.
78. Fritzinger, B.; Capek, R. K.; Lambert, K.; Martins, J. C.; Hens, Z., Utilizing Self-Exchange To Address the Binding of Carboxylic Acid Ligands to CdSe Quantum Dots. *Journal of the American Chemical Society* **2010,** 132, (29), 10195-10201.
79. Williams, D. B. G.; Lawton, M., Drying of Organic Solvents: Quantitative Evaluation of the Efficiency of Several Desiccants. *The Journal of Organic Chemistry* **2010,** 75, (24), 8351-8354.
80. Okada, Y.; Ishikawa, K.; Maeta, N.; Kamiya, H., Understanding the Colloidal Stability of Nanoparticle–Ligand Complexes: Design, Synthesis, and Structure–Function Relationship Studies of Amphiphilic Small-Molecule Ligands. *Chemistry – A European Journal* **2018,** 24, (8), 1853-1858.
81. Bennett, E.; Greenberg, M. W.; Jordan, A. J.; Hamachi, L. S.; Banerjee, S.; Billinge, S. J. L.; Owen, J. S., Size Dependent Optical Properties and Structure of ZnS Nanocrystals Prepared from a Library of Thioureas. *Chemistry of Materials* **2022,** 34, (2), 706-717.
82. Dhaene, E.; Van Driessche, I.; De Buysser, K.; Van Hecke, K., Crystal structures of three N,N,N'-trisubstituted thioureas for reactivity-controlled nanocrystal synthesis. *Acta Crystallographica Section E* **2022,** 78, (2).
83. Hamachi, L. S.; Jen-La Plante, I.; Coryell, A. C.; De Roo, J.; Owen, J. S., Kinetic Control over CdS Nanocrystal Nucleation Using a Library of Thiocarbonates, Thiocarbamates, and Thioureas. *Chemistry of Materials* **2017,** 29, (20), 8711-8719.
84. Akoka, S.; Barantin, L.; Trierweiler, M., Concentration Measurement by Proton NMR Using the ERETIC Method. *Analytical Chemistry* **1999,** 71, (13), 2554-2557.

85. Silvestre, V.; Goupry, S.; Trierweiler, M.; Robins, R.; Akoka, S., Determination of Substrate and Product Concentrations in Lactic Acid Bacterial Fermentations by Proton NMR Using the ERETIC Method. *Analytical Chemistry* **2001,** 73, (8), 1862-1868.
86. Connell, M. A.; Bowyer, P. J.; Adam Bone, P.; Davis, A. L.; Swanson, A. G.; Nilsson, M.; Morris, G. A., Improving the accuracy of pulsed field gradient NMR diffusion experiments: Correction for gradient non-uniformity. *Journal of Magnetic Resonance* **2009,** 198, (1), 121-131.
87. Maes, J.; Castro, N.; De Nolf, K.; Walravens, W.; Abécassis, B.; Hens, Z., Size and Concentration Determination of Colloidal Nanocrystals by Small-Angle X-ray Scattering. *Chemistry of Materials* **2018,** 30, (12), 3952-3962.